Shape-Tension Coupling Produces Nematic Order in an Epithelium Vertex Model

Jan Rozman,[1,*] Julia M. Yeomans,[1] and Rastko Sknepnek[2,3]
[1]Rudolf Peierls Centre for Theoretical Physics, University of Oxford, Oxford OX1 3PU, United Kingdom
[2]School of Science and Engineering, University of Dundee, Dundee DD1 4HN, United Kingdom
[3]School of Life Sciences, University of Dundee, Dundee DD1 5EH, United Kingdom

(Received 2 February 2023; revised 26 June 2023; accepted 20 October 2023; published 27 November 2023)

We study the vertex model for epithelial tissue mechanics extended to include coupling between the cell shapes and tensions in cell-cell junctions. This coupling represents an active force which drives the system out of equilibrium and leads to the formation of nematic order interspersed with prominent, long-lived +1 defects. The defects in the nematic ordering are coupled to the shape of the cell tiling, affecting cell areas and coordinations. This intricate interplay between cell shape, size, and coordination provides a possible mechanism by which tissues could spontaneously develop long-range polarity through local mechanical forces without resorting to long-range chemical patterning.

DOI: 10.1103/PhysRevLett.131.228301

Introduction.—Epithelial tissues are prime examples of dense, active, viscoelastic materials [1–3]. Understanding their behavior is also of fundamental importance in biology since epithelia line organs and cavities in the body, and the majority of cancers develop in epithelial cells [4]. The vertex model [5–7] has played an important role in modeling epithelial mechanics. It can capture the solid-to-fluid transition observed in experiments [8] by tuning its geometric parameters [9]. It is also straightforward to extend it to include active effects, both as self-propulsion [10,11] and as cell junction activity [12–19].

Nematiclike features at scales that span several cells have recently been observed in experiments on epithelial sheets [20–23], and confluent layers of fibroblast [24,25] and myoblast [26] cells. These are a readout of elongated cell shapes, and the defects associated with the nematic state have been argued to play important biological roles, e.g., as sites of cell extrusions [20]. Theories of active nematics [27–31] have been developed that offer explanations for observed collective behaviors in epithelial cell monolayers [32] and bacterial suspensions [33].

Cell motion is, however, not always turbulent, and instead one observes coordinated motion over distances much larger than the typical cell size. Such coordinated movements are key, e.g., during embryonic development [34–36]. One of the central open questions is how these motions are generated, sustained, and regulated. A closely related question is to what extent such large-scale features require guidance by biochemical patterning, e.g., via spatiotemporal coordination of morphogens, or whether they can spontaneously emerge as a result of cellular behaviors. It is, therefore, important to understand how cell-level processes coordinate to form tissue- and organ-scale structures.

It has recently been shown that coupling between tension and a global nematic field leads to active T1 transitions that drive tissue shape changes and can elongate cells [19]. In this Letter, we explore how nematic order can emerge in a vertex model by introducing coupling between the local cell shape, a proxy for the nematic director, and the tension on cell-cell junctions. We find that this model also leads to prominent +1 defects in the nematic order. We primarily focus on the role of these defects in determining local cell shapes and tissue tiling.

Model.—We begin with the vertex model for planar epithelia [5–7] in dimensionless form. The dynamics of the vertices is described by overdamped equations of motion,

$$\dot{\mathbf{r}}^{(i)} = -\nabla_{\mathbf{r}^{(i)}} e_{\mathrm{VM}} + \mathbf{f}^{(i)}_{\mathrm{act}}. \tag{1}$$

Here, $\mathbf{r}^{(i)}$ is the position of the ith vertex, the overdot denotes the time derivative, $\nabla_{\mathbf{r}^{(i)}}$ indicates the gradient with respect to $\mathbf{r}^{(i)}$, e_{VM} is the energy, and $\mathbf{f}^{(i)}_{\mathrm{act}}$ is the active force on the vertex due to coupling between cell shape and junctional tension. The explicit form of $\mathbf{f}^{(i)}_{\mathrm{act}}$ is discussed below. The energy reads

$$e_{\mathrm{VM}} = \sum_c \left[\left(a^{(c)} - 1\right)^2 + k_p\left(p^{(c)} - p_0\right)^2\right], \tag{2}$$

where the sum is over all cells, $a^{(c)}$ and $p^{(c)}$ are, respectively, the area and perimeter of the cell c, k_p is

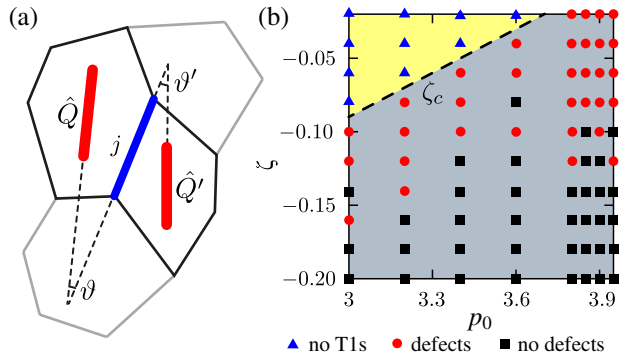

FIG. 1. (a) Schematic representation of the model. Thick red lines are cell directors. The tension of a junction (blue line) depends on its alignment with the directors of the cells sharing the junction. (b) State diagram at $t = 4 \times 10^5$. The dashed line indicates ζ_c.

the perimeter elasticity modulus, whereas p_0 is the target cell-shape index. Parameter p_0 controls the mechanical response of the passive model, with the threshold value between the solid and fluid phases reported in the range ≈3.8–3.9 [9,37–39].

The active force takes the form

$$\mathbf{f}_{\mathrm{act}}^{(i)} = -\sum_j \gamma^{(j)}(t) \nabla_{\mathbf{r}^{(i)}} l^{(j)}, \tag{3}$$

where the sum is over all cell-cell junctions, $\gamma^{(j)}(t)$ is the tension of the jth junction at time t, and $l^{(j)}$ is its length. The tension in a junction evolves according to

$$\dot{\gamma}^{(j)}(t) = -\frac{1}{\tau_\gamma}\left[\gamma^{(j)}(t) - \gamma_0^{(j)}\right], \tag{4}$$

where τ_γ sets a characteristic relaxation timescale and $\gamma_0^{(j)}$ is its target tension. Here, it is selected to couple the tension in the junction with the elongation of its neighboring cells, by choosing

$$\gamma_0^{(j)} = -\frac{1}{2}\zeta[\cos(2\vartheta) + \cos(2\vartheta')]. \tag{5}$$

ϑ and ϑ' are the angles between junction j and the directors of its neighboring cells c and c' [Fig. 1(a)], and ζ is a coupling constant. The sign of ζ determines whether the active forces act to extend or contract a junction that is aligned with the cell's director. We define a cell's director to point along the eigenvector corresponding to the largest eigenvalue of the cell's gyration tensor, given as $\mathbf{G}^{(c)} = (1/n^{(c)}) \sum_{i \in \mathcal{V}_c} (\mathbf{r}^{(i)} - \mathbf{r}_0^{(c)}) \otimes (\mathbf{r}^{(i)} - \mathbf{r}_0^{(c)})$. Here, the sum is over the $n^{(c)}$ vertices of the cell c, and $\mathbf{r}_0^{(c)} = (1/n^{(c)}) \sum_{i \in \mathcal{V}_c} \mathbf{r}^{(i)}$, is the position of the cell's geometric center. Cells for which $\mathbf{G}^{(c)}$ has two identical eigenvalues do not contribute to Eq. (5). We, therefore, distinguish two types of order, cell arrangement measured by the average number of neighbors each cell has and the nematic texture accessed through $\mathbf{G}^{(c)}$. Note that cells in the vertex model are not hard rods, and can deform in such a way that the director changes discontinuously by going through an isotropic intermediary shape for which $\mathbf{G}^{(c)}$ has two identical eigenvalues and, therefore, no director. This may affect local topological charge conservation.

The choice of the coupling between the cell geometry and junction tensions is key for making the system active. Namely, the active force cannot be written as a gradient of a line tension contribution to the energy, which would lead to the dynamics of the system corresponding to passive energy minimization. Instead, the tensions $\gamma^{(j)}$ are coupled to the instantaneous geometry through Eqs. (4) and (5), but the resulting forces are *only* along the junctions. The movement of the vertices they produce can and does change the tissue shape in such a way that the coupling in Eq. (5) further increases the energy because angles ϑ and ϑ' have changed. This is qualitatively different from inserting $\gamma_0^{(j)}$ from Eq. (5) directly into an energy of the form $\gamma_0^{(j)} l^{(j)}$, in which case the gradient would lead to additional terms that would rotate junctions, and the model tissue would relax toward a local energy minimum. Effectively, the gradient does not "know" that the angles ϑ and ϑ' are included in the line tension. As a result, the movement of the vertices does not minimize the energy, rendering the system active. Figure S3a [41] shows an example of how the energy of the model tissue changes in time.

We solve Eq. (1) using the first-order Euler scheme with the time step $\delta t = 0.01$, and we set $k_p = 0.02$ and $\tau_\gamma = 1$. We start simulations with a perturbed hexagonal lattice. We used a 32×32 lattice of cells placed in a periodic simulation box. The longest simulations were run until $t_{\max} = 4 \times 10^5$. Finally, we implemented T1 transitions [40] on junction that fall below a threshold length $l_0 = 0.01$ and have decreased in length since the previous time step. A T1 transition always results in previously separated cells becoming neighbors, and the tension of the new junction is set to 0. See Supplemental Material Sec. II [41] for additional model details.

Results.—We focus on the case of negative ζ, i.e., when junctions aligned with local cell elongation are under a higher tension, as it leads to more interesting physics. The $\zeta > 0$ case is discussed in Supplemental Material Sec. VI [41]. For $\zeta < 0$, we can distinguish three scenarios [Fig. 1(b) and Supplemental Material Sec. III [41]]. (1) Above a threshold value ζ_c, i.e., for $\zeta > \zeta_c$, activity is too weak to rearrange cells. (2) For $\zeta < \zeta_c$, activity induces enough T1 transitions to reorganize the initial tiling and the tissue assumes a nematiclike configuration with locally aligned cells. Defects in the nematic order remain

throughout the entire simulation run (Movie S1 [41]). See Supplemental Material Sec. IV [41] for details of defect detection [42–44]. (3) As ζ decreases further, all nematic defects annihilate, leading to a defect-free nematic order at long times (Fig. S1 and Movies S2, S3). Cells become more motile with decreasing ζ, as quantified by the mean-squared displacement (MSD) defined in Supplemental Material Sec. II [41]. This motion is transient and stops over time, but all tissues with global nematic order have MSD above ten (Supplemental Material, Figs. S3c and S3g [41]), indicating that on average each cell traveled distances of at least three cell diameters. For low p_0, the latter two scenarios still have high average cell-shape indices $q^{(c)} = p^{(c)}/\sqrt{a^{(c)}}$ (Supplemental Material, Figs. S3d and S3h [41]), usually associated with fluid behavior. However, Ref. [38] shows that the relation between $q^{(c)}$ and fluidization also depends on cell alignment for elongated cells. Finally, $|\zeta_c|$ decreases with increasing p_0. Nevertheless, the almost unbroken initial tiling remains for sufficiently small $|\zeta|$ for all studied p_0 values (Fig. S2 [41]).

A striking feature of the cell configurations is the presence of prominent, vortexlike $+1$ nematic defects where cells form concentric rings around the defect core [Figs. 2(a) and 2(b), and Supplemental Material, Figs. S1a and S1c [41]]. This is unexpected since nematic order is typically associated with half-integer defects. The $+1$ defects are ubiquitous and appear for all parameter sets for which cells in the tissue do not remain six-coordinated. Half-integer nematic defects are also present (Supplemental Material, Figs. S1a and S1c [41]) and take part in the annihilation of $+1$ defects. While -1 defects are observed, they are less common than $+1$ defects, and we did not find any prominent behavior relating to them.

The origin of $+1$ defects can be understood as follows. The $\zeta < 0$ case favors high tension in junctions that are aligned with the cell director. This leads to the formation of concentric circles of high-tension junctions around vortexlike $+1$ defects [Fig. 2(a)] that constrict the defect core. To quantify this, we define the angle ϕ of a junction relative to the $+1$ defect core, chosen so that $\phi = 0$ corresponds to a junction that is perpendicular to a circle centered on the defect and going through the middle of the junction, whereas $\phi = \pi/2$ corresponds to a junction tangent to that circle. In Fig. 2(c) we show how the correlation of the angle ϕ and the junction tension changes as a function of distance from the defect core (see Supplemental Material Sec. V [41]). As a result of the concentric circles of high-tension junctions, cells close to the core of a nematic vortexlike $+1$ defect are compressed compared to the cells further away, and the area elasticity balances the tensions [Figs. 2(b) and 2(d)]. The formation of high-tension circles and compression around $+1$ defects are robust to changes in p_0 and ζ [Figs. 2(e) and 2(f)]. They offer a plausible explanation for the long life of $+1$ defects, as the circles of high-tension junctions prevent a $+1$ defect from splitting into a pair of

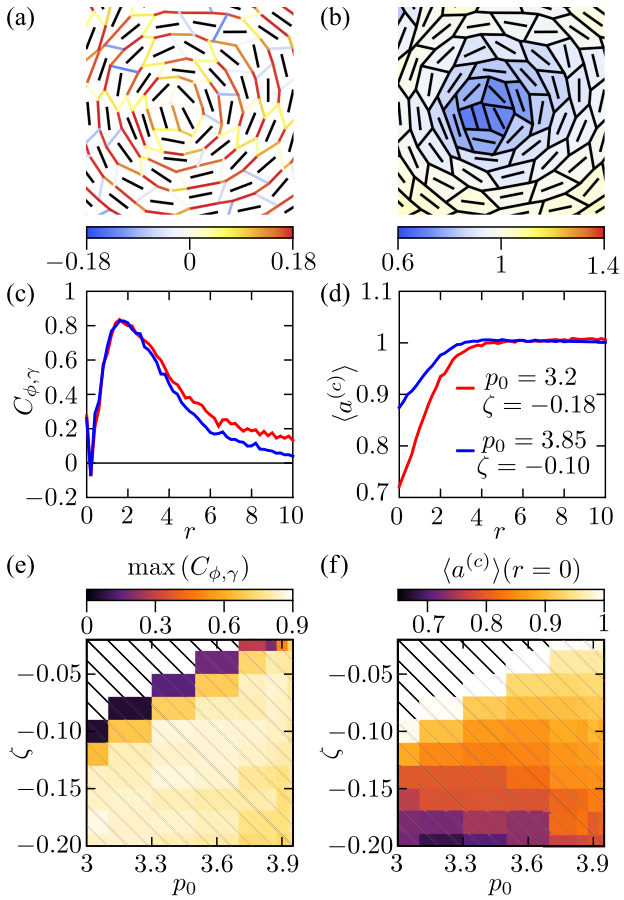

FIG. 2. (a),(b) Close-up of a $+1$ nematic defect for a model tissue with $p_0 = 3.2$, $\zeta = -0.18$ at $t = 1000$. Coloring as follows: (a) junctions according to the tension due to shape-tension coupling or (b) cells according to the cell area. Cell directors are shown in black on both panels. (c),(d) Dependence on distance r from the core of a $+1$ defect of (c) angle-tension correlation function, $C_{\phi,\gamma}(r)$ (see Supplemental Material Sec. V [41]), or (d) average cell area; shown for $t = 1000$. Parameter sets are shown in the inset of panel (d); both parameter sets are in the regime where defect-free nematic order emerges over time. (e) Maximum value of angle-tension correlation function, $C_{\phi,\gamma}(r)$ as a function of p_0 and ζ. (f) The mean area of cells within a circle of radius 0.2 surrounding a $+1$ defect core as a function of p_0 and ζ. Data for (e) and (f) averaged over all $+1$ defects in 40 simulation runs at $t = 1000$. Dashed regions on panels (e) and (f) correspond to parameter sets where activity is too weak to induce T1 transitions.

$+1/2$ defects. Moreover, tissues described by the passive vertex model featuring only area and perimeter elasticity [Eq. (2)] allow for disordered nematic configurations without an associated energy penalty in the fluid phase (Supplemental Material, Fig. S5a [41]). This implies that the passive vertex model does not contain terms analogous to the Frank free energy that penalise gradients in the direction of elongation, which enables long-lived $+1$ nematic defects. To illustrate this, we ran simulations where active forces were turned off after $+1$ defects

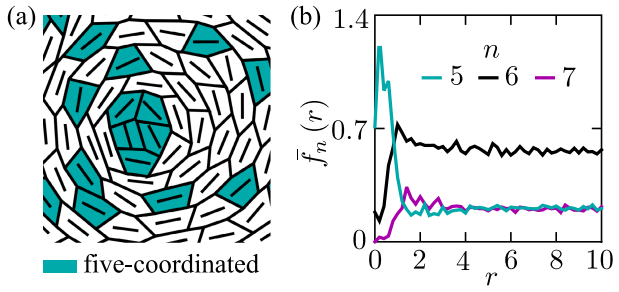

FIG. 3. (a) Close-up of a +1 nematic defect for a model tissue with $p_0 = 3.2$, $\zeta = -0.18$ at $t = 1000$ (i.e., in a regime where defect-free nematic order emerges over time): cells with five neighbors in cyan, other cells in white. (b) Dependence on distance r from the core of a +1 defect of the distribution of 5-, 6-, and 7-sided cells, averaged over 40 simulations and for a bin size $\Delta r = 0.2$ for $p_0 = 3.2$, $\zeta = -0.18$.

emerged and then allowed the system to passively relax. +1 nematic defects persisted even in the passive model (Supplemental Material, Figs. S5b and S5c [41]). While this does not exclude a Frank free energy term arising from coarse graining the model, on the cell level scale, it does not appear to play a significant role. Creation and stability of +1 defects is, therefore, a consequence of the cell geometry and the elastic energy of the vertex model, as well as activity.

The global nematic order contrasts with typical hydrodynamic active nematic models, which are unstable to either bend or splay deformations [27]. To show the absence of a similar active nematic instability, we performed simulations starting from a perturbed but globally ordered configuration. After $t = 10^6$ the global order did not break (Supplemental Material, Fig. S6 [41]). A plausible reason for this difference is that the passive part of the dynamics is not necessarily equivalent to the usual set of nematodynamic equations (e.g., the director does not directly enter into the equations of motion); the active forces are also not identical to those generated by the nematic activity. Moreover, the dynamics are dry (i.e., friction dominated).

The nematic order couples back to the cell tiling through +1 defects. In particular, we find that cells with five neighbors are very common in the vicinity of the +1 defect cores [Fig. 3(a)]. To quantify this, we computed the distribution function,

$$f_n(r) = \frac{1}{n_{+1}} \sum_{d=1}^{n_{+1}} \frac{N_n^{(d)}(r)}{\pi([r+\Delta r]^2 - r^2)}, \tag{6}$$

where the sum is over all $n_{+1} + 1$ defects in a simulated tissue, and $N_n^{(d)}(r)$ is the number of n-sided cells at distances between r and $r + \Delta r$ from +1 defect d. The normalization was chosen such that the two-dimensional integral of the function gives the number of n-sided cells in the model tissue. The resulting plots of averaged $f_n(r)$ are shown in Figs. 3(b) and Supplemental Material, Figs. S4f and S4g [41]. Interestingly, both +1 defects [26,45] and five-neighbor cells [46–48] in the tiling have previously been reported as connected to the formation of budded structures in 3D tissues, so their colocation in our model may be relevant, though typically the experimentally reported +1 defects leading to budding are of the aster type. Last, we note that the position of +1 defects also affects the measured cell-shape index $q^{(c)}$ (Figs. S4b, S4c, S4e and Sec. V in Supplemental Material [41]).

Summary and discussion.—In this Letter, we analyzed a vertex model extended to include coupling between the elongation of cells and junctional tensions, leading to an active force on the vertices. For sufficiently high activity magnitudes, the model tissue forms nematic ordering of elongated cells which, surprisingly, features prominent vortexlike +1 defects. Experimentally, +1 defects have been reported both *in vitro* [49] and *in vivo* [50,51]. It has also been recently argued that +1 defects play a role in morphogenesis [26,45].

Defects in the nematic order are coupled to the tiling of the confluent tissue. Cells around the +1 defects arrange themselves in such a way that the defects are surrounded by nearly concentric circles of high-tension junctions. This leads to the compression of cells near the defect cores. Moreover, cells that form the defect cores often have five neighbors.

To check how general the emergence of long-lived +1 defects and global nematic order are, we tested whether these features remain the same following (i) changing the T1 threshold value, (ii) changing the definition of the cell elongation [42], and (iii) the target active tension also depending on the extent of cell elongations (see Supplemental Material Sec. VII [41]). All three modifications still lead to the emergence of +1 defects. Cases (i) and (ii) also allow for global order, whereas in case (iii), global order emerges if the modified definition of cell elongation from (ii) is used. This implies that the features of the model are generic.

An alternative way to introduce active dipolar forces into the vertex model has been proposed in Ref. [19]. The key difference to our approach is that tensions in our model are coupled directly to the local elongation of cells, rather than to an external, uniform nematic field. This allows the active tensions to reorient the nematic field to which they are coupled and does not require global patterning to drive the formation of nematic order. Furthermore, recent studies have proposed mechanisms by which nematic order can also arise due to polar fluctuating forces [43,52] or due to coupling between the direction of the cell elongation and the direction of self-propulsion [53]. Moreover, it has been demonstrated that extensile behavior can arise in a purely contractile system due to anisotropic fluctuations [54]. Such mechanisms could provide insights into the behavior of epithelial monolayers on a substrate.

Introducing nematic activity into the vertex model can also be achieved via an active stress term proportional to the **Q** tensor. This results in different active forces on vertices and leads to both tissue fluidization and $\pm 1/2$ nematic defects, for sufficiently high activity [42].

Regarding the effects of noise that are inherently present in all biological systems, the movement of cells in our model arises directly from the shape-tension coupling [Eqs. (4) and (5)] and does not rely on noise modeled as an Ornstein-Uhlenbeck process used, e.g., in Refs. [12,15,19], so a noise term was omitted.

The collective behaviors explored here arise from a specific coupling between cell shape and junctional tension. It is important to ask how such coupling could arise in real tissues. There is evidence that cells can sense their shape [55]. In, e.g., the fly, large-scale chemical patterning of cytoskeletal molecules is observed [56–58] that gives global directionality to the tissue, making the model of Duclut *et al.* [19] applicable. On the other hand, in systems such as early-stage avian embryos [35], there is no such global patterning, yet local anisotropy of cell shapes and actomyosin orientation is apparent, albeit with no clear nematic order. It is, therefore, plausible to consider a scenario in which a cell can locally inform its junctions about its current direction.

We wish to thank Mehrana R. Nejad and Guanming Zhang for insightful discussions, and Matej Krajnc for providing the initial version of the vertex model code. J. R. and J. M. Y. acknowledge support from the UK EPSRC (Award No. EP/W023849/1). R. S. acknowledges support from the UK EPSRC (Award No. EP/W023946/1).

*jan.rozman@physics.ox.ac.uk

[1] W. Xi, T. B. Saw, D. Delacour, C. T. Lim, and B. Ladoux, Nat. Rev. Mater. **4**, 23 (2019).
[2] R. Alert and X. Trepat, Phys. Today **74**, No. 6, 30 (2021).
[3] S. Shankar, A. Souslov, M. J. Bowick, M. C. Marchetti, and V. Vitelli, Nat. Rev. Phys. **4**, 380 (2022).
[4] R. A. Weinberg, *The Biology of Cancer* (Garland Science, New York, 2013).
[5] H. Honda and G. Eguchi, J. Theor. Biol. **84**, 575 (1980).
[6] R. Farhadifar, J.-C. Röper, B. Aigouy, S. Eaton, and F. Jülicher, Curr. Biol. **17**, 2095 (2007).
[7] A. G. Fletcher, M. Osterfield, R. E. Baker, and S. Y. Shvartsman, Biophys. J. **106**, 2291 (2014).
[8] J.-A. Park, J. H. Kim, D. Bi, J. A. Mitchel, N. T. Qazvini, K. Tantisira, C. Y. Park, M. McGill, S.-H. Kim, B. Gweon *et al.*, Nat. Mater. **14**, 1040 (2015).
[9] D. Bi, J. Lopez, J. M. Schwarz, and M. L. Manning, Nat. Phys. **11**, 1074 (2015).
[10] D. Bi, X. Yang, M. C. Marchetti, and M. L. Manning, Phys. Rev. X **6**, 021011 (2016).
[11] D. L. Barton, S. Henkes, C. J. Weijer, and R. Sknepnek, PLoS Comput. Biol. **13**, e1005569 (2017).
[12] S. Curran, C. Strandkvist, J. Bathmann, M. de Gennes, A. Kabla, G. Salbreux, and B. Baum, Dev. Cell **43**, 480 (2017).
[13] M. Krajnc, S. Dasgupta, P. Ziherl, and J. Prost, Phys. Rev. E **98**, 022409 (2018).
[14] M. F. Staddon, K. E. Cavanaugh, E. M. Munro, M. L. Gardel, and S. Banerjee, Biophys. J. **117**, 1739 (2019).
[15] M. Krajnc, Soft Matter **16**, 3209 (2020).
[16] R. Sknepnek, I. Djafer-Cherif, M. Chuai, C. J. Weijer, and S. Henkes, eLife **12**, e79862 (2023).
[17] C. Duclut, J. Paijmans, M. M. Inamdar, C. D. Modes, and F. Jülicher, Cells Dev. **168**, 203746 (2021).
[18] T. Yamamoto, D. M. Sussman, T. Shibata, and M. L. Manning, Soft Matter **18**, 2168 (2022).
[19] C. Duclut, J. Paijmans, M. M. Inamdar, C. D. Modes, and F. Jülicher, Eur. Phys. J. E **45**, 29 (2022).
[20] T. B. Saw, A. Doostmohammadi, V. Nier, L. Kocgozlu, S. Thampi, Y. Toyama, P. Marcq, C. T. Lim, J. M. Yeomans, and B. Ladoux, Nature (London) **544**, 212 (2017).
[21] H. Morales-Navarrete, H. Nonaka, A. Scholich, F. Segovia-Miranda, W. de Back, K. Meyer, R. L. Bogorad, V. Koteliansky, L. Brusch, Y. Kalaidzidis *et al.*, eLife **8**, e44860 (2019).
[22] J. Eckert, B. Ladoux, L. Giomi, and T. Schmidt, bioRxiv (2022).
[23] J.-M. Armengol-Collado, L. N. Carenza, J. Eckert, D. Krommydas, and L. Giomi, Nat. Phys. (2023).
[24] G. Duclos, S. Garcia, H. Yevick, and P. Silberzan, Soft Matter **10**, 2346 (2014).
[25] G. Duclos, C. Erlenkämper, J.-F. Joanny, and P. Silberzan, Nat. Phys. **13**, 58 (2017).
[26] P. Guillamat, C. Blanch-Mercader, G. Pernollet, K. Kruse, and A. Roux, Nat. Mater. **21**, 588 (2022).
[27] R. A. Simha and S. Ramaswamy, Phys. Rev. Lett. **89**, 058101 (2002).
[28] M. Marchetti, J. Joanny, S. Ramaswamy, T. Liverpool, J. Prost, M. Rao, and R. A. Simha, Rev. Mod. Phys. **85**, 1143 (2013).
[29] L. Giomi, Phys. Rev. X **5**, 031003 (2015).
[30] A. Doostmohammadi, J. Ignés-Mullol, J. M. Yeomans, and F. Sagués, Nat. Commun. **9**, 3246 (2018).
[31] S. Thampi and J. M. Yeomans, Eur. Phys. J. Spec. Top. **225**, 651 (2016).
[32] R. Mueller, J. M. Yeomans, and A. Doostmohammadi, Phys. Rev. Lett. **122**, 048004 (2019).
[33] I. S. Aranson, Rep. Prog. Phys. **85**, 076601 (2022).
[34] L. Wolpert, C. Tickle, and A. M. Arias, *Principles of Development* (Oxford University Press, USA, 2015).
[35] E. Rozbicki, M. Chuai, A. I. Karjalainen, F. Song, H. M. Sang, R. Martin, H.-J. Knölker, M. P. MacDonald, and C. J. Weijer, Nat. Cell Biol. **17**, 397 (2015).
[36] J. Gros, K. Feistel, C. Viebahn, M. Blum, and C. J. Tabin, Science **324**, 941 (2009).
[37] M. Merkel, K. Baumgarten, B. P. Tighe, and M. L. Manning, Proc. Natl. Acad. Sci. U.S.A. **116**, 6560 (2019).
[38] X. Wang, M. Merkel, L. B. Sutter, G. Erdemci-Tandogan, M. L. Manning, and K. E. Kasza, Proc. Natl. Acad. Sci. U.S.A. **117**, 13541 (2020).
[39] S. Tong, N. K. Singh, R. Sknepnek, and A. Košmrlj, PLoS Comput. Biol. **18**, e1010135 (2022).

[40] A. G. Fletcher, J. M. Osborne, P. K. Maini, and D. J. Gavaghan, Prog. Biophys. Molec. Biol. **113**, 299 (2013).
[41] See Supplemental Material at http://link.aps.org/supplemental/10.1103/PhysRevLett.131.228301 for Figs. S1–S9, captions for Movies S1–S3, and technical background information, including Refs. [5–7,42–44].
[42] S.-Z. Lin, M. Merkel, and J.-F. Rupprecht, Phys. Rev. Lett. **130**, 058202 (2023).
[43] A. Killeen, T. Bertrand, and C. F. Lee, Phys. Rev. Lett. **128**, 078001 (2022).
[44] A. J. Vromans and L. Giomi, Soft Matter **12**, 6490 (2016).
[45] Y. Maroudas-Sacks, L. Garion, L. Shani-Zerbib, A. Livshits, E. Braun, and K. Keren, Nat. Phys. **17**, 251 (2021).
[46] J. Rozman, M. Krajnc, and P. Ziherl, Nat. Commun. **11**, 3805 (2020).
[47] J. Rozman, M. Krajnc, and P. Ziherl, Eur. Phys. J. E **44**, 99 (2021).
[48] L. A. Hoffmann, L. N. Carenza, J. Eckert, and L. Giomi, Sci. Adv. **8**, eabk2712 (2022).
[49] K. D. Endresen, M. Kim, M. Pittman, Y. Chen, and F. Serra, Soft Matter **17**, 5878 (2021).
[50] T. Bonhoeffer and A. Grinvald, Nature (London) **353**, 429 (1991).
[51] F. Wolf and T. Geisel, Nature (London) **395**, 73 (1998).
[52] F. Vafa, M. J. Bowick, B. I. Shraiman, and M. C. Marchetti, Soft Matter **17**, 3068 (2021).
[53] M. Paoluzzi, L. Angelani, G. Gosti, M. C. Marchetti, I. Pagonabarraga, and G. Ruocco, Phys. Rev. E **104**, 044606 (2021).
[54] G. Zhang and J. M. Yeomans, Phys. Rev. Lett. **130**, 038202 (2023).
[55] A. Haupt and N. Minc, J. Cell Sci. **131**, jcs214015 (2018).
[56] C. Bertet, L. Sulak, and T. Lecuit, Nature (London) **429**, 667 (2004).
[57] F. Bosveld, I. Bonnet, B. Guirao, S. Tlili, Z. Wang, A. Petitalot, R. Marchand, P.-L. Bardet, P. Marcq, F. Graner *et al.*, Science **336**, 724 (2012).
[58] R. J. Tetley, G. B. Blanchard, A. G. Fletcher, R. J. Adams, and B. Sanson, eLife **5**, e12094 (2016).